DEVELOPMENT OF EMPIRICAL AND ANALYTICAL REACTION WHEEL DISTURBANCE MODELS

Rebecca A. Masterson*, David W. Miller† and Robert L. Grogan‡

*†Space Systems Laboratory
Department of Aeronautics and Astronautics
Massachusetts Institute of Technology
Cambridge, MA 02139

‡Jet Propulsion Laboratory
California Institute of Technology
4800 Oak Grove Drive
Pasadena, CA 91109

Abstract

Accurate disturbance models are necessary to predict the effects of vibrations on the performance of precision space-based telescopes, such as the Space Interferometry Mission (SIM). There are many possible disturbance sources on such a spacecraft, but the reaction wheel assembly (RWA) is anticipated to be the largest. The following paper presents two types of reaction wheel disturbance models. A steady-state empirical model which assumes the disturbances consist of discrete harmonics of the wheel speed, and a non-linear analytical model which is developed using energy methods to capture the internal flexibilities and fundamental harmonic of an unbalanced wheel. Experimental data obtained from Ithaco B and E type wheels is used to determine the model parameters for both types of models and a comparison between the models and data is presented. The analytical model is currently a work in progress, but preliminary results indicate that an accurate disturbance model can be constructed by combining features of both the empirical and analytical modeling techniques.

Introduction

Next generation precision space-based telescopes, such as the Space Interferometry Mission (SIM), require high levels of pointing stability. Small levels of vibration can introduce jitter in the optical train and cause a significant reduction in image quality. Vibrations may be induced by mechanical systems and sensors located on the spacecraft, such as cryo-coolers, optical delay lines, and other optical elements. The largest anticipated disturbance source on SIM is the reaction wheel assembly (RWA). Therefore, accurate models of reaction wheel disturbances are necessary to predict their effect on the spacecraft performance and develop methods to control the undesired vibration.

Reaction wheels are momentum exchange devices which are often used for spacecraft attitude control and for performing large angle slewing maneuvers. A typical reaction wheel assembly consists of a rotating flywheel suspended on ball bearings encased in a housing and driven by an internal brushless DC motor.[1] As the wheel spins, disturbances can occur from four main sources: flywheel imbalance, bearing disturbances, motor disturbances and motor driven errors.[2] Flywheel imbalance is generally the largest disturbance source in the reaction wheel and can cause both a disturbance force and torque at the frequency at which the wheel is spinning. This disturbance will be referred to as the fundamental harmonic throughout the remainder of the paper. Bearing disturbances, which are caused by irregularities in the balls, races, and/or cage, produce high frequency disturbances at higher harmonics of the wheel speed.[3] Disturbances from these two sources will be the focus of this paper.

Two different types of reaction wheel models will be discussed. The first is an empirical model which was developed for the Hubble Space Telescope (HST) wheels and is mostly system-ID based. Since every type of RWA will produce slightly different disturbances, a MATLAB toolbox has been developed which extracts the empirical model parameters from steady-state reaction wheel data. However, the test data shows that the RWA also includes internal flexibility which results in amplification of the harmonic disturbances at certain wheel speeds. These effects are not captured by the empirical model. Therefore a second model is created which is more physics based. It is an analytical model which captures the physical behavior of an unbalanced rotating flywheel as wheel as well as the internal flexibility of the wheel.

The following paper will focus on these two RWA disturbance models. First, the empirical model will

*Graduate student, TRW Fellow, *becki@mit.edu*
†Assistant Professor, Director Space Systems Lab, *millerd@mit.edu*
‡Member of Engineering Staff, Jet Propulsion Laboratory, *Robert.L.Grogan@jpl.nasa.gov*

Presented at the 1999 AIAA/ASME/ASCE/AHS/ASC Structures, Structural Dynamics and Materials Conference, St. Louis MO

be presented and the methods used to extract the model parameters from steady-state RWA data discussed. Data taken from Ithaco B and E type wheels will be used to illustrate the process. Then, a preliminary version of the analytical model and the theory used to build it will be presented. Also, the use of experimental data to determine the parameters for this model will be discussed as well, using the Ithaco wheel data as examples. Finally, the empirical and analytical model will be compared to the experimental data and the advantages and disadvantages of each will be discussed. Methods of using the empirical model to improve the analytical model will be explored.

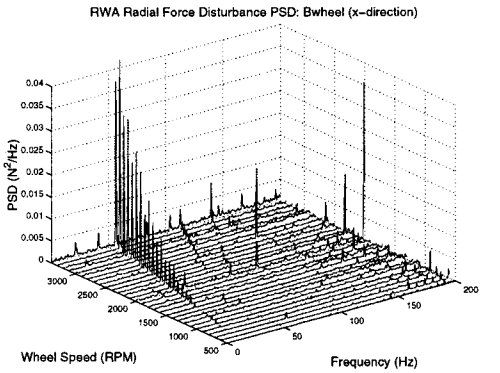

Figure 1: Example Waterfall Plot

Experimental Data

Two sets of reaction wheel data will be used in this paper to illustrate and validate the modeling techniques. The first set was taken at Orbital's Germantown, MD facility and is disturbance data from Ithaco B-type wheels, model TW-16B32. The wheels tested were off-the-shelf engineering and flight unit wheels for the FUSE mission. During testing, the wheels were hard-mounted to a Kistler force/torque table and spun at speeds ranging from 500-3400 rpm at intervals of 100 rpm. Once the wheel had achieved steady-state spin at the desired speed disturbance forces and torques at the mounting interface between the wheel and plate were measured with four 3-axis load cells located in the force/torque table. The data was sampled at 1kHz for $\approx$ 8 seconds with anti-aliasing filters at 480 Hz. The data was processed using MATLAB to obtain the power spectral densities (PSDs) and amplitude spectra of the time histories of the wheel disturbances at each speed. A PSD is a measure of the power in a signal as a function of frequency. It is generally represented in units^2/Hz and the area under a PSD is equal to the variance of the signal. An amplitude spectrum is an estimate of the signal amplitude as a function of frequency. The amplitude spectrum of a force disturbance time signal has units of N and is plotted against frequency. A point on the curve (f, amp) can be considered a sin wave with frequency, f, and amplitude, amp.

Frequency domain data can be plotted side by side in a 3-dimensional plot known as a waterfall plot. An example of a waterfall plot is shown in Figure 1. The data shown is the F_x disturbance data obtained from the B wheel test. The data is only plotted up to 200 Hz because after this point the mode of the test stand corrupts the disturbance data. Note the diagonal ridges in the data. The frequency of these disturbances changes linearly with wheel speed. These disturbances are the wheel harmonics; the largest is the fundamental harmonic.

The second set of test data was taken at the NASA Goddard Space Flight Center using a single Ithaco E-type, off-the-shelf, standard catalog product reaction wheel. The wheel was integrated into a stiff cylindrical test fixture and hard-mounted to a 6-axis Kistler force/torque table. In this test, the wheel was started at 0 rpm and full torque voltage was applied to the motor until the wheel saturated around 2400 rpm. The data was sampled at 3840 Hz for 390 seconds. In order to use the data to obtain a steady-state empirical model of the form shown in Equation 1, the data had to be divided into time slices of 8192 points each. Each of these time slices was considered quasi-steady-state and used to compute the PSD and/or amplitude spectra. Then the resulting frequency domain data was used to estimate the average speed of the wheel during that time slice.[4] When processed in this manner, the E-wheel data could be treated as steady-state data similar to the B-wheel data.

The data from each test consists of 6 disturbances: x-axis force, F_x, y-axis force, F_y, z-axis force, F_z, x-axis torque, T_x, y-axis torque, T_y and z-axis torque, T_z. Since the z-axis is the spin axis of the wheel the F_x and F_y data are both the radial force disturbances and should be nearly identical. Both of these datasets are used to create the radial force disturbance model. Similarly, T_x and T_y are both radial torque data and should also be the same. These datasets are used to create the radial torque model. The F_z data is the axial force data and is used to create the axial force disturbance model. The T_z data is the disturbance torque about the spin axis. This disturbance is very small and can be neglected.

The following section will illustrate how the experimental data is used to determine the model parameters, h_i and C_i, for the empirical model. The B wheel data will be used as an example.

Empirical Model

Similar to SIM, HST had very fine pointing and mechanical stability requirements. Therefore, charac-

terization of RWA vibrations was important to the spacecraft performance, and a disturbance model was developed using the results of induced vibration testing on the HST RWA flight units.[5] The model assumes that the disturbances consist of discrete harmonics of the reaction wheel speed with amplitudes proportional to the square of the wheel speed:

$$m(t) = \sum_{i=1}^{n} C_i f_{rwa}^2 \sin(2\pi h_i f_{rwa} t + \phi_i) \qquad (1)$$

where $m(t)$ is the disturbance force or torque, n is the number of harmonics included in the model, C_i is the amplitude of the ith harmonic, f_{rwa} is the wheel speed in Hz, h_i is the ith harmonic number and ϕ_i is a random phase (assumed to be uniform over $[0, 2\pi]$).[6] Note that this model yields disturbance forces and torques as a function of the wheel speed. Transient effects induced from changing wheel speeds are not included.

Identifying Harmonic Numbers

The first step in the empirical modeling process is to use the experimental data to determine at which ratios of the wheel frequency disturbances occur. These values are called the harmonic numbers, h_i. A MATLAB function has been created which, given steady-state reaction wheel disturbance data for one direction, returns a list of harmonic numbers for that wheel. The function individually examines all the amplitude spectra in the dataset and locates spikes which are due to the harmonic disturbances of the wheel. To illustrate this process we will consider the F_x disturbance of the B wheel dataset.

The B wheel F_x dataset consists of 30 time histories, one taken every 100 rpm from 500-3400 rpm, which were processed into amplitude spectra and PSDs (see Figure 1). The first step in extracting the harmonic numbers from this data is to frequency normalize the data by dividing the frequency vector by the speed at which the wheel was spinning when the data was taken. Figure 2 shows an example at 3400 rpm. The upper plot is the amplitude spectrum plotted vs. frequency. The lower plot shows the same frequency data plotted against the normalized frequency. The x-axis of the lower plot is now non-dimensional. Note that the largest disturbance occurs at the number one. This peak is caused by the fundamental harmonic disturbance.

Once all the amplitude spectra in the dataset are frequency normalized MATLAB searches for peaks in the data at each wheel speed. It is important to note that not all peaks found in the amplitude spectra are a result of harmonic disturbances. Some may be due to noise or side lobes of the harmonics resulting from performing an FFT on the time history data. These noisy spikes are isolated from the disturbance harmonics using a histogram. The

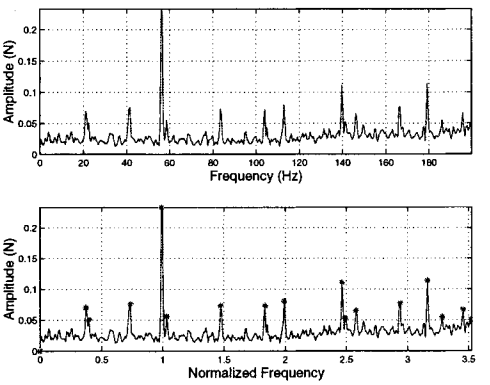

Figure 2: Peak Identification in B Wheel F_x Data at 3400 rpm

peaks are binned according to spike amplitude. The peaks which fall in the largest bin with a small amplitude are considered noise and discarded. The remaining spikes are considered possible harmonic disturbances. The result of this process is illustrated in Figure 2. The stars indicate which spikes were chosen by MATLAB as possible disturbances. Note that the smaller "noisy" spikes are not marked. The locations, or harmonic numbers, of the disturbance spikes are placed into a matrix. All the amplitude spectra in the dataset are searched in this manner until a complete matrix of spike locations, with each column corresponding to a different wheel speed, is built.

A true harmonic disturbance should occur at the same harmonic number in all wheel speeds. Therefore, a binning algorithm is used to search the spike locations matrix for matching harmonic numbers across wheel speeds. Numbers at which spikes occur in more than a given percentage of possible wheel speeds are returned as the harmonic numbers corresponding to that dataset. The radial force and radial torque model harmonic numbers are determined by comparing and combining the harmonic numbers extracted from the F_x and F_y data and the T_x and T_y data, respectively. The axial force harmonic numbers are simply the harmonic numbers extracted from the F_z data.

Calculating Amplitude Coefficients

To complete the empirical model the amplitude coefficients, C_i, must be extracted from the data. A MATLAB function was developed to accomplish this task using the same method employed in the modeling of the HST wheels.[5] The magnitude of the disturbance force (or torque) is assumed to be related to the wheel speed as follows:

$$F_i = C_i \Omega^2 \qquad (2)$$

where F_i is the disturbance force resulting from the ith harmonic in N (or Nm for a torque), C_i is the

amplitude coefficient of the ith harmonic in N/rpm^2 (or Nm/rpm^2), and Ω is the wheel speed in rpm.

Equation 2 is used to calculate the amplitude coefficients by performing a least squares fit on the experimental data. The error between the experimental data and the theory for the ith harmonic at the jth wheel speed, e_{ij} is:

$$e_{ij} = F_{ij} - C_i\Omega_j^2 \tag{3}$$

where F_{ij} is the experimental disturbance force of the ith harmonic in the dataset corresponding to the jth wheel speed, Ω_j. Then, the square of the error (Equation 3) is summed over all wheel speeds and minimized, resulting in the following equation for C_i:

$$C_i = \frac{\sum_j F_{ij}\Omega_j^2}{\sum_j \Omega_j^4} \tag{4}$$

The MATLAB implementation of Equation 4 uses the amplitude spectra of the time domain data to find the actual disturbance force at each harmonic number over all wheel speeds. For example, consider the F_x dataset of the B wheel and the fundamental harmonic, $h_1 = 1.0$. The amplitude coefficient for this harmonic, C_1 is determined by first looping through all 30 amplitude spectra and recording the amplitude of the force at the frequency corresponding to the number 1.0 harmonic at each wheel speed. Then the force data and wheel speeds are summed as shown in Equation 4 to calculate the amplitude coefficient. A disturbance at the ith harmonic may not be visible in all the amplitude spectra in a dataset. For example, harmonic disturbances are more difficult to identify in data taken at low wheel speeds due to a low signal to noise ratio. Therefore, if a disturbance spike could not be detected in the data at a given wheel speed, the force, F_{ij} and speed, ω_j for that wheel speed were not included in the summation of Equation 4.

The results of the curve fit for the 1.0 and 3.87 harmonics of the B wheel data (F_x and F_y) are shown in Figure 3. The circles represent the force amplitudes of the experimental data over the different wheel speeds. Note that some of the circles lie on the x-axis. These points are from wheel speeds in which that particular harmonic disturbance was not visible in the data. The solid line is the curve generated using the calculated C_i and Equation 2. Both the F_x and F_y data were used to perform the curve fit in this case since both directions are radial force data. Therefore, a more accurate radial force amplitude coefficient can be obtained by combining both data sets when performing the analysis.

The coefficient curve fit plots are useful for a number of reasons. First, they show how well the assumption in Equation 2 holds. In Figure 3(a) the data points lay right along the theoretical curve.

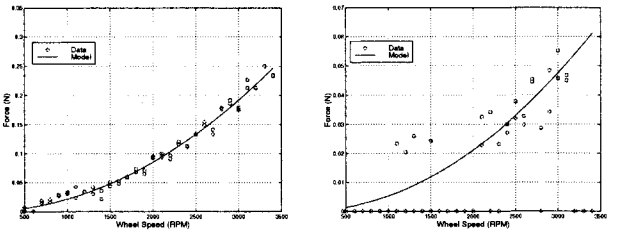

(a) (b)

Figure 3: Amplitude Coefficient Curve Fits for B Wheel Radial Force Data: (a) $h_1 = 1.0$ (b) $h_5 = 3.87$

This result suggests that the assumption of Equation 2 is a good one for the fundamental harmonic. Physics will also be used to support this claim when the analytical model is discussed. In contrast, the curve fit seen in Figure 3(b) is not quite as good. This plot suggests that the assumed force-speed relationship may not hold for the higher harmonics. However, it will provide an estimate of the amplitude coefficients for these harmonics. The curve fit plots can also be used to eliminate harmonics from the model. If the curve fit is not based on enough data points there cannot be a high degree of confidence in the resulting amplitude coefficient. Therefore, these harmonics should be removed from the model due to a lack of data.

In addition, the effects of the internal wheel modes on the harmonic disturbances can be observed in the coefficient curve fits. Figure 4 shows the coefficient curve fit for the second radial force harmonic, $h_2 = 1.99$ of the B wheel. The lighter points and curve are the initial results of the amplitude coefficient calculation. Note that the data points show a large increase in force amplitude between 1300 and 1900 rpm. This amplitude increase occurs when this harmonic cross one of the internal wheel modes. Since this interaction between the harmonics and the wheel modes is not included in the empirical model it should not be included in the calculation of the amplitude coefficient. Therefore, these points were removed from the summation (Equation 4) and the coefficient was recalculated. The darker data points and curve are the results of the second analysis. Note that removing the points affected by the wheel mode has decreased the amplitude coefficient for this harmonic. The interaction between the harmonics and the internal wheel modes will be explored in more detail when the analytical model is discussed.

Model Validation: Comparing to Data

Comparing the model to the experimental data is the final step in the empirical modeling process. Plotting the model against the experimental data allows validation and refinement (if necessary) of the harmonic numbers and amplitude coefficients . Figure 5

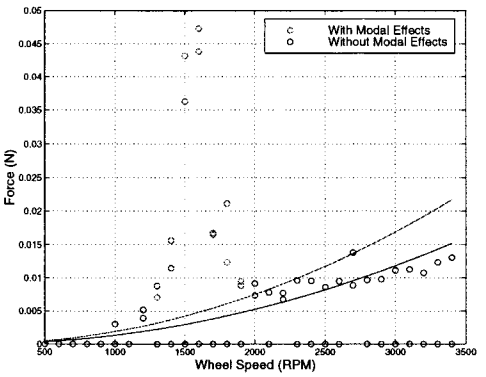

Figure 4: Effects of Internal Wheel Modes on Amplitude Coefficient Curve Fit: $h_2 = 1.99$ (B Wheel Radial Force)

is a waterfall plot of the F_x data PSDs (continuous lines) plotted with the radial force model PSDs (circle). The PSD of the model was derived by finding the autocorrelation, $R_m(\tau)$ of Equation 1 assuming that ϕ_i is a random variable over the interval $[0, 2\pi]$ and that ϕ_i and ϕ_j are statistically independent:

$$R_m(\tau) = \sum_{i=1}^{n} \frac{C_i^2 f_{rwa}^4}{2} \cos(2\pi f_{rwa} h_i \tau) \qquad (5)$$

Then, the one-sided PSD, $S_m(\omega)$, is:[7]

$$S_m(\omega) = \sum_{i=1}^{n} \frac{C_i^2 f_{rwa}^4}{2} \delta(\omega - 2\pi f_{rwa} h_i) \qquad (6)$$

Note that the PSD shown in Equation 6 consists of a series of discrete impulses occurring at frequencies, $f_{rwa}h_i$, with amplitude, $\frac{C_i^2 f_{rwa}^4}{2}$. The data PSDs, however, are continuous over frequency. Therefore, it is important to keep in mind that the model amplitude is actually the variance, or the area under the spike in the PSD, of that harmonic disturbance. This discrepancy makes comparing the disturbance amplitudes on this type of plot difficult. However, the waterfall plot is useful for validating the harmonic numbers. Note in Figure 5 that the diagonal lines of circles lie on top of the diagonal spike ridges seen in the data. This plot indicates that the location of the harmonics have been identified correctly.

Figure 6 allows validation of the amplitude coefficients. The continuous curve in the plot is the amplitude spectra of the F_x data when the wheel was spinning at 3000 rpm. The discrete impulses, marked with circles, are the radial force model (with amplitudes and frequencies from Equation 1) at the same wheel speed. Since the amplitude spectra is simply the amplitude of the disturbance at each frequency the two curves can be compared directly.

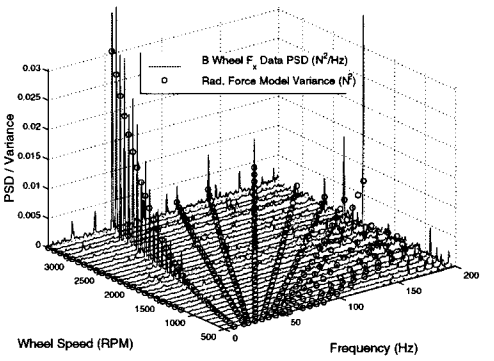

Figure 5: Waterfall Plot Comparison of Radial Force Model to F_x Data (B Wheel)

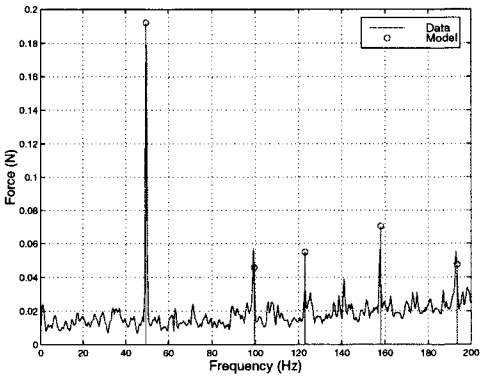

Figure 6: Amplitude Spectra Comparison of Radial Force Model to F_x Data (B Wheel) at 3000 rpm

Note that the amplitude of the first harmonic, which is the fundamental, matches the amplitude of the data quite well. The comparison of the higher harmonics, on the other hand, is not as good. This discrepancy is most likely due to the assumption that the disturbance force is proportional to the wheel speed squared. As mentioned earlier, this assumption seems valid for the fundamental harmonic but begins to break down with the higher harmonics. The plot does indicate, however, that the model provides a reasonable estimate to the data.

Analytical Model

It has been shown that although the empirical model captures the tonal quality of reaction wheel disturbances and provides a good estimate for the location and amplitude of the harmonics it is not an accurate model since it does not include the internal flexibility in the wheel. Figure 4 illustrates the fact that this internal compliance will result in an amplification of the harmonic disturbance at certain wheel speeds. A complete disturbance model should include this interaction between the disturbance harmonics and structural wheel modes. Therefore, a non-linear, an-

alytical model of a reaction wheel which captures some of the structural modes of the wheel and the effects of the fundamental harmonic has been developed.

The internal wheel flexibility was modeled using linear springs and the flywheel imbalance was modeled with lumped masses positioned strategically on the wheel. Energy methods were used to derive the equations of motion of the system. These equations were then simulated using a MATLAB ODE solver and the experimental data was used to fit some of the model parameters. The following sections will present this analytical model. First the structural modes of the wheel will be discussed. Then, the problem of a balanced rotating wheel on flexible supports is solved. Finally, the static and dynamic imbalance masses are added to the flywheel to complete the model.

Internal Wheel Flexibility

The RWA can be modeled as having five degrees of freedom: translation in the axial direction, translation in the two radial directions and rotation about the two radial axes. This model results in three dominant vibrational modes: axial translation, radial translation and rocking. These modes are depicted schematically in Figure 7.[2]

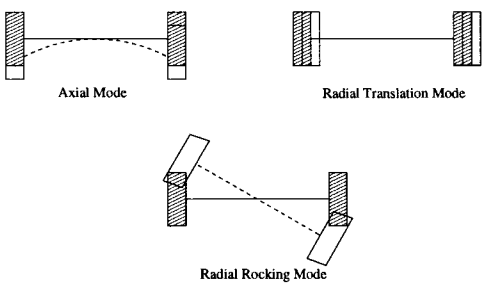

Figure 7: Internal Wheel Modes

The structural wheel modes can be seen in the waterfall plots of the experimental data. They appear as ridges in the PSDs (or amplitude spectra) occurring at a constant frequency across wheel speeds. Figure 8 shows an example of the axial translation mode in the B wheel F_z data. The mode is located at $\approx$ 75 Hz and is highlighted in the plot with a solid line. Note that at 1600 rpm, when a harmonic crosses the mode, there is very large amplification in the disturbance magnitude.

Figure 9 is a plot of the E wheel F_x data in which the radial translation and rocking modes are visible. The radial translation mode occurs at $\approx$ 230 Hz and is also highlighted with a solid line. The amplification of the harmonics crossing this mode can be seen at high wheel speeds. The rocking mode occurs at lower frequencies and behaves differently than the translational modes. It is not constant across wheel speeds, but is a function of wheel speed. In addition,

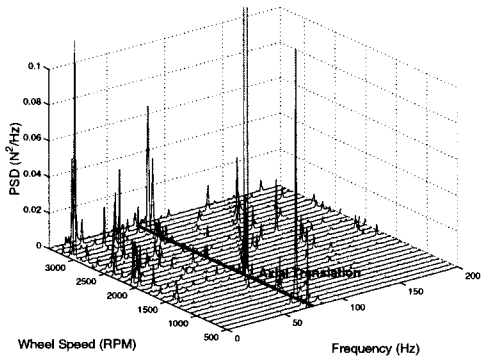

Figure 8: Axial Translation Mode in B Wheel Data

the mode is split into two natural frequencies forming a V-shaped ridge in the data. The frequency of the positive whirl increases with wheel speed while that of the negative whirl decreases. The splitting of this mode is due to gyroscopic effects caused by the spinning of the wheel and will be discussed in more detail in the following section. Amplification of the harmonic disturbance by both whirls of the rocking mode can be best seen in the plot between 1500 and 2000 rpm.

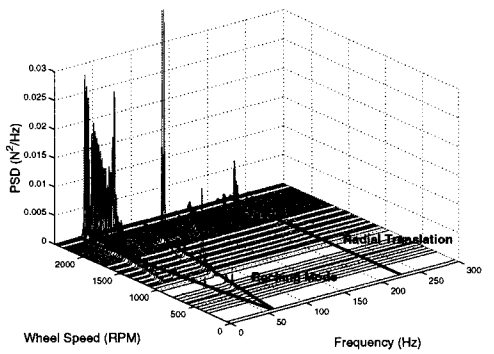

Figure 9: Radial Translation and Rocking Modes in E Wheel Data

Balanced Wheel: Rocking and Radial Modes

The problem of a balanced flywheel on flexible supports is considered first to capture the radial modes (translation and rocking) and gyroscopic stiffening of the wheel. At this stage, the model is axisymmetric so the kinetic energy could be written in the body-fixed reference frame. However, when the dynamic imbalance masses are added, the model becomes asymmetric and the kinetic energy must be written in a ground-fixed reference frame. Therefore, the ground-fixed reference frame will be used here as well.

Figure 10 shows a balanced wheel on flexible supports. The shaft flexibility is modeled by the four linear springs of stiffness $\frac{k}{2}$ located at a distance d from the center of the wheel. The ground-fixed reference frame is **XYZ** and the shaft-fixed, non-rotating

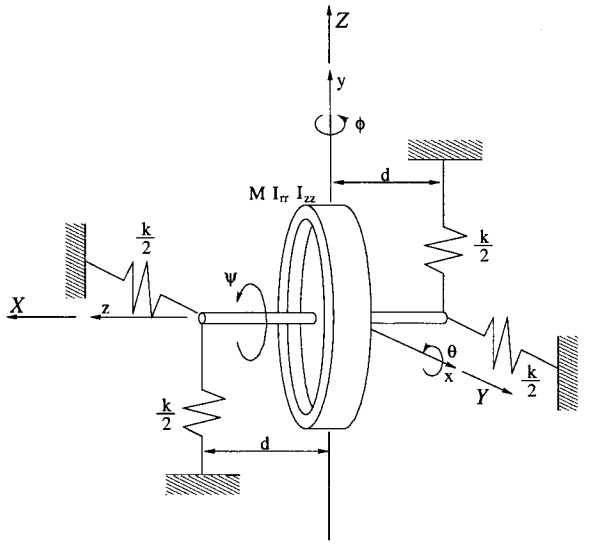

Figure 10: Model of Balanced Flywheel on Flexible Supports

frame is **xyz**. The wheel has mass, M, radius, R, and principal moments of inertia I_{rr} and I_{zz}, where:

$$I_{rr} = \frac{1}{2}MR^2 \quad (7)$$

$$I_{zz} = \frac{1}{4}MR^2 \quad (8)$$

The model has four generalized coordinates, x, y, θ and ϕ. x and y are the radial translation of the wheel along the **Y** and **Z** axes, and θ and ϕ are the rotations of the wheel about these axes, respectively. The wheel is also free to spin about the shaft-fixed **z**-axis with constant angular velocity, $\dot{\psi}$. Euler angles and coordinate transformations are used to write the angular velocity of the balanced wheel in the ground-fixed reference frame:

$$\omega_{\mathbf{XYZ}} = (\dot{\psi}\cos\theta\cos\phi - \dot{\theta}\sin\phi)U_{\mathbf{X}} + (\dot{\theta}\cos\phi + \dot{\psi}\cos\theta\sin\phi)U_{\mathbf{Y}} + (\dot{\phi} - \dot{\psi}\sin\theta)U_{\mathbf{Z}} \quad (9)$$

The mass moments of inertia of the wheel in the ground-fixed frame can be calculated in terms of its principal moments of inertia, I_{rr} and I_{zz}:

$$I_{\mathbf{XX}} = I_{rr}(1 + \cos^2\phi\cos^2\theta) \quad (10)$$

$$I_{\mathbf{XY}} = I_{rr}\cos\phi\sin\phi\cos^2\theta \quad (11)$$

$$I_{\mathbf{XZ}} = -I_{rr}\cos\phi\sin\theta\cos\theta \quad (12)$$

$$I_{\mathbf{YY}} = I_{rr}(1 + \sin^2\phi\cos^2\theta) \quad (13)$$

$$I_{\mathbf{YZ}} = -I_{rr}\sin\phi\sin\theta\cos\theta \quad (14)$$

$$I_{\mathbf{ZZ}} = I_{zz}(1 - \frac{1}{2}\cos^2\theta) \quad (15)$$

Equations 9-15 are used to write the kinetic energy of the balanced wheel in the inertial, ground-fixed reference frame:

$$T_{wheel} = \frac{1}{2}[(\dot{\theta}^2 + \dot{\phi}^2(1 + \sin^2\theta))I_{rr} + (\dot{\psi}^2 - 2\dot{\phi}\dot{\psi}\sin\theta)I_{zz} + M(\dot{x}^2 + \dot{y}^2)] \quad (16)$$

The potential energy is, by inspection:

$$V = \frac{k}{4}[(x + d\sin\phi)^2 + (x - d\sin\phi)^2 + (y + d\sin\theta)^2 + (y - d\sin\theta)^2] \quad (17)$$

However, since the wheel is centered axially on the shaft, Equation 17 reduces to:

$$V = \frac{k}{2}[d^2(\sin^2\theta + \sin^2\phi) + x^2 + y^2] \quad (18)$$

The equations of motion are derived using Equations 16 and 18 and Lagrangian methods. They are linearized by assuming small motion about x, y, ϕ and θ. The translational and rotational degrees are freedom are decoupled in this case (due to the assumed symmetry in the model) and can be considered separately:

$$\begin{bmatrix} M & 0 \\ 0 & M \end{bmatrix}\begin{Bmatrix} \ddot{x} \\ \ddot{y} \end{Bmatrix} + \begin{bmatrix} k & 0 \\ 0 & k \end{bmatrix}\begin{Bmatrix} x \\ y \end{Bmatrix} = \mathbf{0} \quad (19)$$

Substituting $\dot{\psi} = \Omega$ for the constant wheel speed:

$$\begin{bmatrix} I_{rr} & 0 \\ 0 & I_{rr} \end{bmatrix}\begin{Bmatrix} \ddot{\theta} \\ \ddot{\phi} \end{Bmatrix} + \begin{bmatrix} 0 & \Omega I_{zz} \\ -\Omega I_{zz} & 0 \end{bmatrix}\begin{Bmatrix} \dot{\theta} \\ \dot{\phi} \end{Bmatrix} + \begin{bmatrix} kd^2 & 0 \\ 0 & kd^2 \end{bmatrix}\begin{Bmatrix} \theta \\ \phi \end{Bmatrix} = \mathbf{0} \quad (20)$$

These equations of motion can be used to determine the natural frequencies of the balanced wheel. Solving for the eigenvalues in Equation 19 yields the following frequency for the two transverse vibrational modes:

$$\omega_T = \sqrt{\frac{k}{M}} \quad (21)$$

This frequency is the natural frequency of the radial translation mode of the wheel.

The frequencies of the rotational modes are found by assuming that the solutions to Equation 20 are of the form, $\theta = Ae^{i\omega t}$ and $\phi = Be^{i\omega t}$. Substituting in Equation 20 and solving for ω gives two rotational natural frequencies:

$$\omega_{1,2} = \mp\frac{\Omega I_{zz}}{2I_{rr}} + \sqrt{\left(\frac{\Omega I_{zz}}{2I_{rr}}\right)^2 + \frac{kd^2}{I_{rr}}} \quad (22)$$

Note that $\omega_{1,2}$ are dependent on the spin rate of the wheel, Ω. The gyroscopic precession of the flywheel

and the flexibility of the shaft creates a rocking mode which splits into the two frequencies shown in Equation 22. For the first mode, the whirl is opposed to the rotation of the wheel and destiffens as the wheel speed increases. For the second mode, the whirl and the wheel rotation are in the same direction and a stiffening of the mode results with increasing wheel speed.[8]

Static Imbalance

The balanced wheel and flexible shaft model (Figure 10) captures the radial translation and rocking modes of the wheel. The static imbalance must now be added to model the radial force disturbances of the rotating wheel. Static imbalance is the offset of the center of mass of the wheel from the axis of rotation. It is most easily modeled as a small mass, m_s, placed at a radius, r_s, on the wheel as shown in Figure 11.[2]

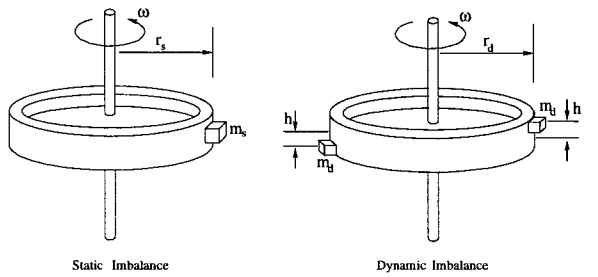

Figure 11: Models of Static and Dynamic Wheel Imbalances

The kinetic energy of the static imbalance mass is derived by first determining the position of the mass on the wheel in the inertial, ground-fixed reference frame, **XYZ** (see Figure 12):

$$\begin{aligned} R_{m_s} &= r_s(\sin\phi\sin\psi + \cos\phi\sin\theta\cos\psi)U_{\mathbf{X}} \\ &+ (r_s(\sin\phi\cos\psi\sin\theta - \cos\phi\sin\psi) + x)U_{\mathbf{Y}} \\ &+ (r_s\cos\theta\cos\psi + y)U_{\mathbf{Z}} \end{aligned} \quad (23)$$

Then, the kinetic energy can be written by differentiating the three components of Equation 23 to obtain the velocity of the mass, v_{m_s}, and using $T = \frac{1}{2}\mathbf{v}^T m\mathbf{v}$:

$$\begin{aligned} T_{m_s} &= \frac{m_s}{2}[2r_s^2\dot{\phi}(\dot{\theta}\cos\theta\cos\psi\sin\psi - \dot{\psi}\sin\theta) \\ &+ r_s^2(\dot{\phi}^2(1-\cos^2\psi\cos^2\theta) + \dot{\theta}^2\cos^2\psi + \dot{\psi}^2) \\ &+ r_s\dot{x}(2\dot{\phi}(\sin\phi\sin\psi + \cos\phi\sin\theta\cos\psi) \\ &- 2\dot{\psi}(\cos\phi\cos\psi - \sin\phi\sin\theta\sin\psi) \\ &+ 2\dot{\theta}\sin\phi\cos\psi\cos\theta) - 2r_s\dot{y}(\dot{\theta}\sin\theta\cos\psi \\ &+ \dot{\psi}\cos\theta\sin\psi) + \dot{x}^2 + \dot{y}^2] \end{aligned} \quad (24)$$

A new kinetic energy is derived by combining Equation 24 and Equation 16. The resulting kinetic energy is then used along with Equation 18 and Lagrangian methods to derive the equations of motion for the new system. After linearizing as described above and substituting $\dot{\psi} = \Omega$ and $\psi = \Omega t$ it can be seen that the addition of the static imbalance to the model results in a driving term in the translational equations of motion which is proportional to the wheel speed, Ω, squared:

$$\begin{bmatrix} M+m_s & 0 \\ 0 & M+m_s \end{bmatrix}\begin{Bmatrix} \ddot{x} \\ \ddot{y} \end{Bmatrix} + \begin{bmatrix} k & 0 \\ 0 & k \end{bmatrix}\begin{Bmatrix} x \\ y \end{Bmatrix} = m_s r_s \Omega^2 \begin{Bmatrix} \sin\Omega t \\ -\cos\Omega t \end{Bmatrix} \quad (25)$$

Recall that the rotational and translational degrees of freedom are decoupled for this model. Therefore, the addition of the static imbalance mass does not affect the rotational degrees of freedom.

Dynamic Imbalance

The dynamic imbalance is added to the model using methods similar to those used to incorporate the static imbalance. Physically, dynamic imbalance is caused by the angular misalignment of the principal axis of the wheel and the spin axis. It is modeled as two equal masses, m_d, placed 180° apart at a radial distance, r_d, and an axial distance, h from the center of the flywheel as shown in Figure 11.[2] In this model, the dynamic imbalance creates the radial torque disturbances of the rotating wheel.

The position of the two masses in the inertial, ground-fixed reference frame, **XYZ**, must first be determined. These vectors are found through inspection and the use of coordinate transformations:

$$\begin{aligned} R_{m_{d1}} &= (r_d(\sin\phi\sin\psi + \cos\phi\sin\theta\cos\psi) \\ &+ h\cos\phi\cos\theta)u_{\mathbf{X}} + (r_d(\sin\phi\cos\psi\sin\theta \\ &- \cos\phi\sin\psi) + h\cos\theta\sin\phi + x)u_{\mathbf{Y}} \\ &+ (r_d\cos\theta\cos\psi - h\sin\theta + y)u_{\mathbf{Z}} \end{aligned} \quad (26)$$

$$\begin{aligned} R_{m_{d2}} &= (-r_d(\sin\phi\sin\psi + \cos\phi\sin\theta\cos\psi) \\ &- h\cos\phi\cos\theta)u_{\mathbf{X}} + (-r_d(\sin\phi\cos\psi\sin\theta \\ &- \cos\phi\sin\psi) - h\cos\theta\sin\phi + x)u_{\mathbf{Y}} \\ &+ (-r_d\cos\theta\cos\psi + h\sin\theta + y)u_{\mathbf{Z}} \end{aligned} \quad (27)$$

Now, the velocity of the dynamic imbalance masses, $v_{m_{d1}}$ and $v_{m_{d2}}$, can be derived by simply differentiating Equations 26 and 27. Then the kinetic energy added to the system by the dynamic imbalance masses is simply:

$$T_{m_d} = \frac{1}{2}\mathbf{v_{m_{d1}}}^T m_d \mathbf{v_{m_{d1}}} + \frac{1}{2}\mathbf{v_{m_{d2}}}^T m_d \mathbf{v_{m_{d2}}} \quad (28)$$

Differentiating and substituting gives:

$$T_{m_d} = m_d[\dot{x}^2 + \dot{y}^2 + (r_d^2\cos^2\psi + h^2)\dot{\theta}^2 + (h^2\cos^2\theta$$

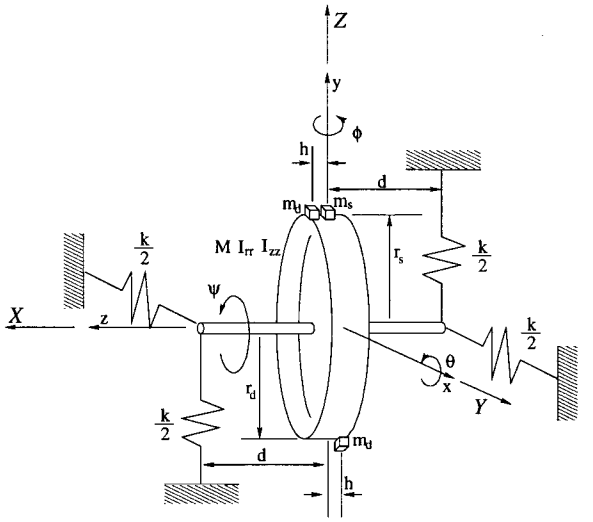

Figure 12: Analytical RWA Model

$$+ r_d^2(1-\cos^2\psi\cos^2\theta) + r_d h\cos\psi\sin(2\theta))\dot{\phi}^2 + r_d^2\dot{\psi}^2 + 2r_d\dot{\theta}\sin\psi(h\dot{\psi} + (r_d\cos\psi\cos\theta - h\sin\theta)\dot{\phi}) - 2r_d\dot{\phi}\dot{\psi}(r_d\sin\theta + h\cos\psi\cos\theta)] \quad (29)$$

All elements are now incorporated in the model and the full equations of motion can be obtained.

Full Model

The full model is shown in Figure 12. Its kinetic energy is simply the sum of the kinetic energy of the balanced wheel (Equation 16), the kinetic energy of the static imbalance mass (Equation 24), and the kinetic energy of the dynamic imbalance masses (Equation 29):

$$T = T_{wheel} + T_{m_s} + T_{m_d} \quad (30)$$

The Lagrangian is formed using the total kinetic energy of the system and the potential energy derived above (Equation 18). The equations of motion of the reaction wheel are then obtained by differentiating the Lagrangian.

Again, the translational and rotational degrees of freedom are perfectly decoupled in this case and can be considered separately. The equations of motion for the translational degrees of freedom, x and y, are:

$$\begin{bmatrix} M_{tot} & 0 \\ 0 & M_{tot} \end{bmatrix} \begin{Bmatrix} \ddot{x} \\ \ddot{y} \end{Bmatrix} + \begin{bmatrix} k & 0 \\ 0 & k \end{bmatrix} \begin{Bmatrix} x \\ y \end{Bmatrix} = m_s r_s \Omega^2 \begin{Bmatrix} \sin\Omega t \\ -\cos\Omega t \end{Bmatrix} \quad (31)$$

where:

$$M_{tot} = M + m_s + 2m_d \quad (32)$$

The equations of motion for the rotational degrees of freedom, θ and ϕ, are:

$$\begin{bmatrix} I_{eff_\theta} & \frac{1}{2}I_{iz}\sin 2\Omega t \\ \frac{1}{2}I_{iz}\sin 2\Omega t & I_{eff_\phi} \end{bmatrix} \begin{Bmatrix} \ddot{\theta} \\ \ddot{\phi} \end{Bmatrix} + \Omega \begin{bmatrix} -I_{iz}\sin 2\Omega t & I_{zz} + 2I_{iz}\cos^2\Omega t \\ -I_{zz} - 2I_{iz}\sin^2\Omega t & I_{iz}\sin 2\Omega t \end{bmatrix} \begin{Bmatrix} \dot{\theta} \\ \dot{\phi} \end{Bmatrix} + \begin{bmatrix} kd^2 & 0 \\ 0 & kd^2 \end{bmatrix} \begin{Bmatrix} \theta \\ \phi \end{Bmatrix} = -2m_d r_d h\Omega^2 \begin{Bmatrix} \cos\Omega t \\ \sin\Omega t \end{Bmatrix} \quad (33)$$

$$I_{eff_\theta} = I_{rr} + 2m_d h^2 + (m_s r_s^2 + 2m_d r_d^2)\cos^2\Omega t \quad (34)$$

$$I_{eff_\phi} = I_{rr} + 2m_d h^2 + (m_s r_s^2 + 2m_d r_d^2)\sin^2\Omega t \quad (35)$$

$$I_{iz} = 2m_d r_d^2 + m_s r_s^2 \quad (36)$$

A MATLAB ODE solver, such as ode45, can be used along with these equations to drive the wheel at some velocity, Ω, and obtain the time response of the model.

Conclusions and Future Work

A method for creating an empirical model of reaction wheel disturbances from steady-state reaction wheel test data has been developed. This type of model captures the tonal quality of reaction wheel disturbances and provides reasonable estimates for the frequencies and amplitudes of the wheel harmonics. Data from Ithaco B and E type wheels have been used to validate the model. However, the experimental data shows that the internal flexibility of the wheel has an effect on the disturbances. When a wheel harmonic crosses a structural mode there is a considerable amplification in the disturbance. The empirical model does not account for this effect. Therefore, an analytical model was developed which includes the radial modes of the wheel (translation and rocking) and the fundamental harmonic. The exciting of the structural modes by the fundamental harmonic is captured in this model. The model parameters control the frequencies of the structural modes, the amplitude of the fundamental harmonic, and the amplification of the harmonic by the structural modes. The values of these parameters are determined from the experimental data.

The analytical model is a work in progress. The axial mode of the wheel must be incorporated before it can be considered complete. In addition, it is important to note that although the analytical model captures the effects of the structural wheel modes on the disturbances it only does so for the fundamental harmonic. The higher harmonics, which are observed in the data and captured in the empirical model, are not represented. This discrepancy suggests that the most accurate disturbance model is

a combination of the empirical and the analytical models. Such a model would use the harmonic numbers and amplitude coefficients extracted from the experimental data by the empirical modeling process to add the higher harmonics into the analytical model. As a result the interactions between the structural wheel modes and all the wheel harmonics would be captured.

Acknowledgments

Part of the work described in this paper was conducted at the Massachusetts Institute of Technology under contract from the Jet Propulsion Laboratory, California Institute of Technology (Contract Number 961-123), with Dr. Sanjay S. Joshi as contract monitor. Part of the work described in this paper was carried out at the Jet Propulsion Laboratory, California Institute of Technology, under contract with the National Aeronautics and Space Administration.

References

[1] Bailke, B., "High Fidelity Mathematical Modeling of Reaction Wheel Performance," in *21st Annual American Astronautical Society Guidance and Control Conference*, February 1998. AAS paper 98-063.

[2] Bialke, B., "A Compilation of Reaction Wheel Induced Spacecraft Disturbances," in *20th Annual American Aeronautical Society Guidance and Control Conference*, February 1997. AAS paper 97-038.

[3] Li, B., G. Goddu, and M.-Y. Chow, "Detection of Common Motor Bearing Faults Using Frequency-Domain Vibration Signals and a Neural Network Based Approach," in *Proceedings of the American Control Conference*, June 1998.

[4] de Weck, O., "Reaction Wheel Disturbance Analysis." MIT SSL Memo, October 1998.

[5] Hasha, M. D., "Reaction Wheel Mechanical Noise Variations." Space Telescope Program Engineering Memo SSS 218, June 1986.

[6] Melody, J. W., "Discrete-Frequency and Broadband Reaction Wheel Disturbance Models." JPL Interoffice Memo #3411-95-200csi (Internal Document), June 1995.

[7] Wirsching, P. H., T. L. Paez, and H. Ortiz, *Random Vibrations: Theory and Practice*, John Wiley & Sons, Inc., 1995.

[8] Ehrich, F. F., ed., *Handbook of Rotordynamics*, McGraw-Hill, Inc., 1992.